ADVANCED FUNCTIONAL MATERIALS
www.afm-journal.de

Silver/Reduced Graphene Oxide Hydrogel as Novel Bactericidal Filter for Point-of-Use Water Disinfection

*Xiangkang Zeng, David T. McCarthy, Ana Deletic, and Xiwang Zhang**

Nanomaterials open an alternative way for water disinfection. However, limitations such as aggregation, toxicity, and complex post-treatment block their practical application. In this study, an antibacterial silver/reduced graphene oxide (Ag/rGO) hydrogel consisting of controlled porous rGO network and well-dispersed Ag nanoparticle is synthesized by a facile hydrothermal reaction. Scanning electron microscopy, transmission electron microscope, X-ray diffraction, mercury porosimetry, and Fourier transform IR spectroscopy are employed to characterize the Ag/rGO hydrogel. The 3D structure of the rGO network serves as an excellent support for Ag nanoparticles. Disinfection experiments show that the Ag/rGO hydrogel exhibits good efficacy against *Escherichia coli* when used as a bactericidal filter driven by gravity. The mechanistic study indicates that bacteria cells are inactivated due to cell membrane damage induced by silver nanoparticles and rGO nanosheets when they flow through Ag/rGO hydrogel. Moreover, due to the retaining of Ag by rGO, the leaching level of silver from Ag/rGO hydrogel is considerably lower than the drinking water standard. This study sheds new light on designing antibacterial materials for point-of-use water disinfection application.

1. Introduction

Contamination of pathogenic microorganisms in impaired water has become a critical issue with deep social, sanitary, and economic impact.[1] Every year pathogen-contaminated water causes more than two million deaths, most of which are children under the age of five.[2] Typically, in the aftermath of natural disasters, or in rural areas where access to conventional water disinfection infrastructure is inadequate and water quality is variable, portable point-of-use (POU) water disinfection technologies are essential.[3] Recently, antimicrobial nanomaterials have drawn increasing attention to water treatment, showing promising application for POU disinfection. Because antimicrobial nanomaterials do not consume any chemicals or energy during the operation, they can be applied as POU water disinfection technology to supply safe drinking water.[4] Among various nanomaterials, silver (Ag) nanoparticles exhibit superior antimicrobial performances. However, Ag nanoparticles readily aggregate in water impairing their performance and are also difficult to separate from treated water. Hence, it is more practical to immobilize them on a substrate, so that the problems of aggregation and post-treatment can be overcome.[5]

Graphene and its derivatives, graphene oxide (GO) and reduced graphene oxide (rGO), being one of the most widely researched 2D nanomaterials are an ideal substrate for the growth and retaining of nanoparticles on its surface.[6] In addition, the newly discovered GO and rGO nanosheets can also inactivate bacteria due to the damage to their cell membranes through physical and chemical interactions.[7–9] This opens a new application of graphene for water disinfection, considering its antimicrobial activity, high mechanical strength, high surface area, and controllable hydrophilic–lipophilic balance.[10] However, the bacterial inactivation induced by graphene is slow, often taking several hours for complete inactivation.[7] Such slow inactivation rate would limit its practical application. Most recently, a few studies have ensued to incorporate Ag nanoparticles with rGO and results show that Ag/rGO composites can achieve more effective, swift disinfection than Ag or rGO alone, due to the synergistic effects between rGO and Ag nanoparticles.[11] Although Ag/rGO composite possesses enhanced antibacterial activity, the two key challenges hindering its application in water disinfection still remain unsolved. So far, Ag/rGO composites in most previous studies are powdery nanosized materials.[11] Due to high surface area, which is one of the key reasons for the high antimicrobial activity, powdery nanomaterials readily aggregate in aqueous solution.[12] Another challenge is that an efficient downstream separation process is still necessary after disinfection reaction to separate powdery Ag/rGO nanomaterials from the treated water. Separating nanosized materials from water is always costly because of their small sizes.[12] Hence, Ag/rGO composite with macroscopic structure is highly needed for water disinfection.

Assembling nanostructured materials into macroscopic devices, which translates nanoscale processes to a macroscopic

X. Zeng, Prof. X. Zhang
Department of Chemical Engineering
Monash University
Clayton, Victoria 3800, Australia
E-mail: xiwang.zhang@monash.edu
Dr. D. T. McCarthy, Prof. A. Deletic
Environmental and Public Health Microbiology Laboratory (EPHM Lab)
Monash Water for Liveability
Department of Civil Engineering
Monash University
Clayton, Victoria 3800, Australia

DOI: 10.1002/adfm.201501454

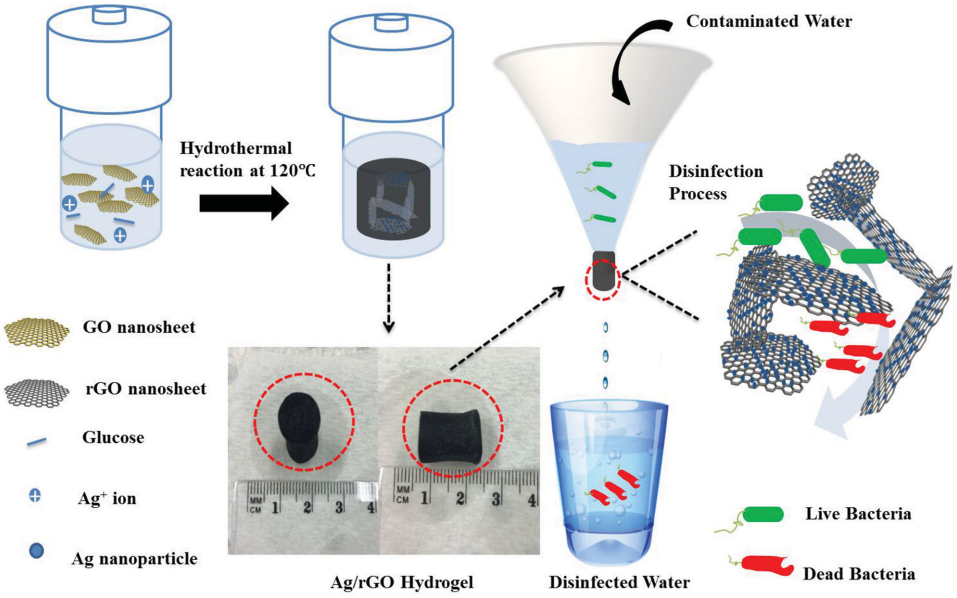

Figure 1. Illustration of the synthesis and application of Ag/rGO hydrogel as bactericidal filter for point-of-use water disinfection.

level, is considered essential for realizing the full potential of nanomaterials.[13,14] Through different methods, GO nanosheets can form macroscopic porous hydrogels, while at the same time retaining the beneficial attributes.[15] Recently, many graphene hydrogels have been fabricated and used as supercapacitors,[16] fixed bed catalytic reactors,[14] stimuli-responsive actuators,[17] cellular scaffolds,[18] and wound dressing agents.[19] However, limited work has been done on applying graphene-based hydrogels for water disinfection.

In the present work, a facile method is developed for the synthesis of a novel Ag/rGO hydrogel with controlled porous rGO network and dispersed Ag nanoparticles. As illustrated in **Figure 1**, the Ag/rGO hydrogel is formed via a one-pot hydrothermal reaction using the mixture of GO nanosheets, glucose, and $AgNO_3$ as precursors. The Ag/rGO hydrogels synthesized under different conditions are characterized to understand the formation mechanism. The hydrogels are then applied as bactericidal filters for water disinfection, driven only by gravity. Moreover, the morphological changes of bacteria cells after filtration are investigated to understand the bactericidal mechanism of the Ag/rGO hydrogels.

2. Results and Discussion

2.1. Characterization of Ag/rGO Hydrogel

As shown in Figure 1, the size of the synthesized cylindrical Ag/rGO hydrogel is 10 mm in diameter and 15 mm in height, which are governed by the autoclave size. **Figure 2**a–c shows the scanning electron microscopy (SEM) images of the Ag/rGO hydrogel (freeze dried), revealing its high porosity. As indicated in Figure 2a,b, the diameter of the pores in Ag/rGO hydrogel is around 5 μm. Moreover, the pore walls consist of thin layers of rGO (Figure 2c). Transmission electron microscope (TEM) images of Ag/rGO (Figure 2d,e) illustrate that Ag nanoparticles of 5–20 nm are almost homogeneously grafted onto the surface of rGO. The lattice fringes in the high-resolution TEM (HRTEM) image of the Ag/rGO hydrogel (Figure 2f) signify the crystallinity of Ag nanoparticles and the distance between two fringes was measured to be 0.231 nm, which accords with the (111) plane of Ag.[20] **Figure 3**a represents the X-ray diffraction (XRD) patterns of GO, rGO, and Ag/rGO. Before hydrothermal reaction, GO shows a typical diffraction peak at around 9.8°, corresponding to the (002) diffraction peak. After hydrothermal reaction, this peak shifts to around 24.0°, which is attributed by the fact that GO nanosheets are

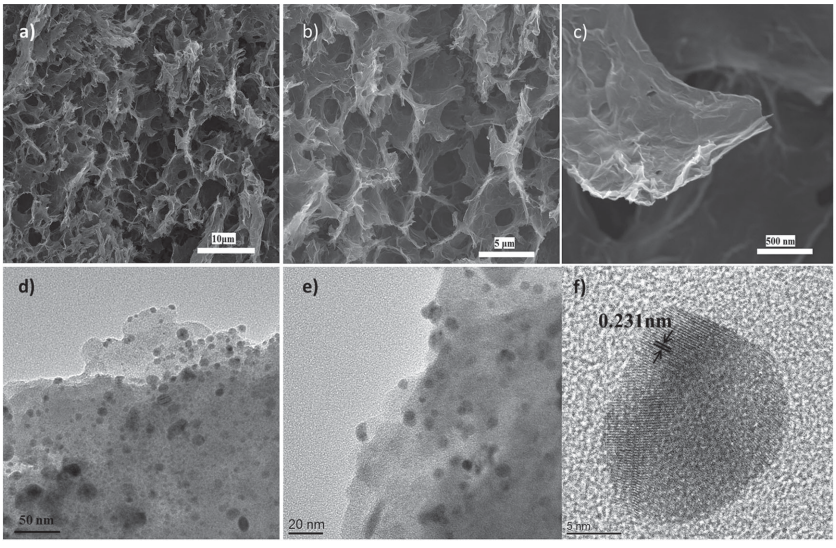

Figure 2. a–c) SEM images and d–f) TEM images of Ag/rGO hydrogel.

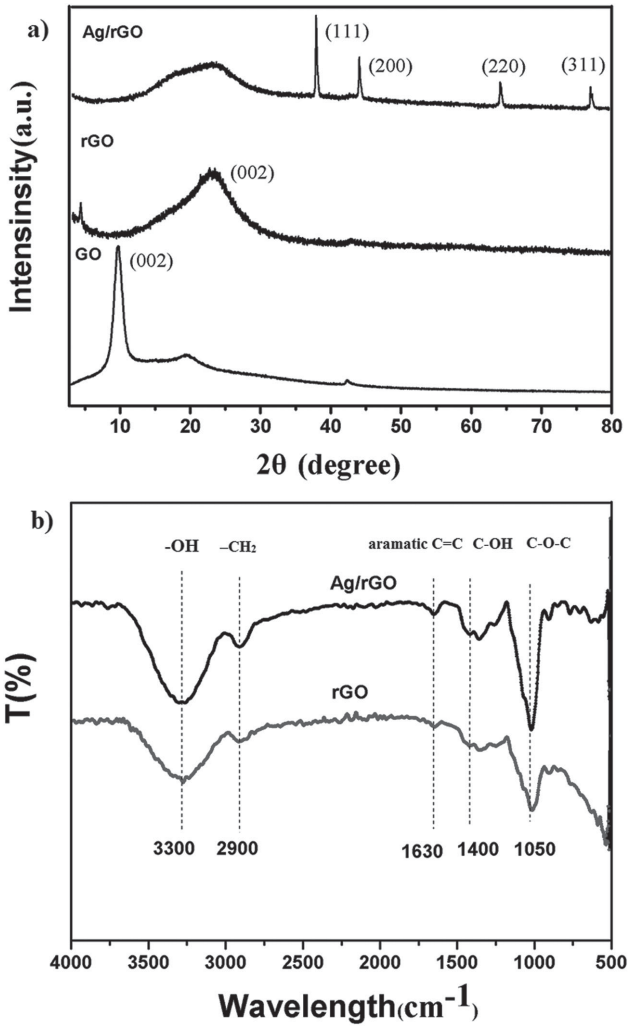

Figure 3. a) XRD patterns of GO, rGO, and Ag/rGO and b) FTIR spectra of rGO and Ag/rGO.

partially reduced and restacked during the hydrothermal process.[19] For Ag/rGO hydrogel, embedded Ag nanoparticles are further evidenced by the concerted peaks at $2\theta = 38.1°$, 44.2°, 64.5°, and 77.5°, which are indexed to the (111), (200), (220), and (311) diffractions of metallic Ag, respectively (JCPDS No. 04-0783).[21] The Fourier transform infrared (FTIR) spectra of Ag/rGO and pure rGO hydrogels both show absorption peaks at around 3300, 2900, 1630, 1400, and 1050 cm^{-1} (Figure 3b), corresponding to the O—H stretching vibration, —CH_2 stretching vibration, skeletal vibration of graphitic skeleton, C—OH, and C—O—C stretching vibration, respectively.[22] This indicates that GO nanosheets are partially reduced during the hydrothermal reaction. In the one-pot hydrothermal reaction, Ag^+ in the precursor is firstly adsorbed to the GO surface via the electrostatic interaction between Ag^+ and the oxygen-containing groups of GO.[23] The adsorbed ions and GO are then simultaneously reduced by glucose. The in-situ reduced Ag nanoparticles on rGO could further form nanocrystal at high temperature. During the crystallization process, as studied by Wang et al.,[24] the pinning force provided by the functional oxygen groups of GO hinders the movement and recrystallization of the formed nanocrystals on rGO substrate. Thus, the oxygen groups of Ag/rGO hydrogel provide good anchoring positions for the growth of Ag nanocrystals on rGO nanosheet.

To verify the role of Ag nanoparticles on the synthesis of the Ag/rGO hydrogel, a series of Ag/rGO hydrogels were synthesized at different $AgNO_3$/GO ratios in the precursor and then characterized by SEM and TEM. As shown in **Figure 4**a, the porosity of pure rGO hydrogel without Ag is low and some rGO nanosheets are closely packed, forming thick layers. When the mass ratio of $AgNO_3$/GO increases to 0.17:1, rGO nanosheets begin to interconnect each other and form a porous structure. However, there are still some compacted graphene layers (Figure 4b). At the ratio of 0.5:1, a porous graphene hydrogel with a thin wall is obtained (Figure 4c). However, further increasing the ratio of $AgNO_3$/GO from 0.5:1 to 2:1 does not create a more porous structure, but leads to the formation of some large and aggregated Ag particles on rGO nanosheets (Figure S1, Supporting Information). Figure S2 (Supporting Information) reveals that the pore size distributions of rGO hydrogel and Ag/rGO hydrogel are different. rGO hydrogel exhibits a wide pore size distribution (0.1–4 μm), which centered at 2.283 μm. By contrast, Ag/rGO hydrogel has larger pores centered at 5.713 μm and narrower pore size distribution although it still varies widely. Moreover, the pore area of Ag/rGO hydrogel (619.8 $m^2\ g^{-1}$) derived from mercury porosimetry is also higher than that of rGO hydrogel (389.1 $m^2\ g^{-1}$). This indicates that Ag nanoparticles facilitate the formation of larger pore and higher porosity in Ag/rGO hydrogel.

It has been previously reported that graphene hydrogels can be prepared via hydrothermal reduction from GO suspension via the π–π stacking between the rGO sheets and the absorption of water molecule by the residual oxygenated functional groups on rGO.[25] For the rGO hydrogel, a closely packed layer is formed, which accords with other studies in the literature. This shows that the preferential rearrangement of the exfoliated GO nanosheet is face-to-face.[14] Different from that in rGO hydrogel, the Ag nanoparticles could serve as the active sites for the assembling of rGO nanosheets in Ag/rGO hydrogel. Since there are corrugations formed in the Ag-bearing rGO nanosheet, the assembly of rGO sheets by Ag particles would further form porous structures (Figure 2). Thus, it can be concluded that the Ag nanoparticles on rGO nanosheets promote the forming of the porous Ag/rGO hydrogel, which is consistent with the method demonstrated by Tang et al.[14] In addition, glucose in the precursor is also necessary in the formation of Ag/rGO hydrogel, as it not only reduces the aggregation of Ag nanoparticles but also increases the mechanical strength of the Ag/rGO hydrogel as shown in Figure S3, Supporting Information.

2.2. Water Disinfection by Ag/rGO Hydrogel

The antibacterial ability of the prepared hydrogels was first assessed by disc diffusion method. As shown in Figure S4 (Supporting Information), the inhibition zone of Ag/rGO hydrogel is clearer than that of pure rGO hydrogel, which indicates Ag/rGO hydrogel exhibits better bacterial inactivation capability

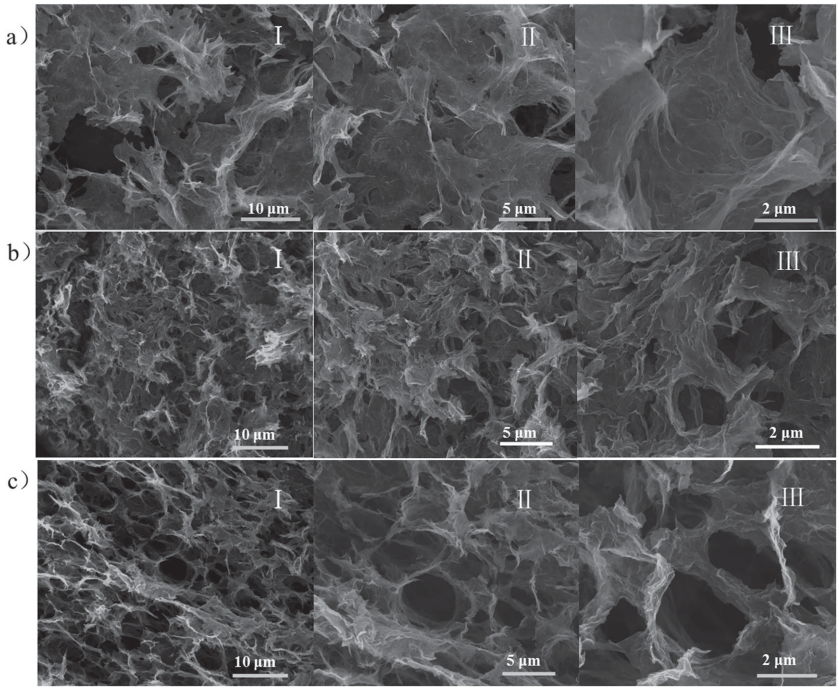

Figure 4. SEM images of Ag/rGO hydrogels prepared at different mass ratio of $AgNO_3$/GO. a) $AgNO_3$/GO = 0:1, b) $AgNO_3$/GO = 0.17:1, and c) $AgNO_3$/GO GO = 0.5:1. The mass of GO in all samples is 30 mg.

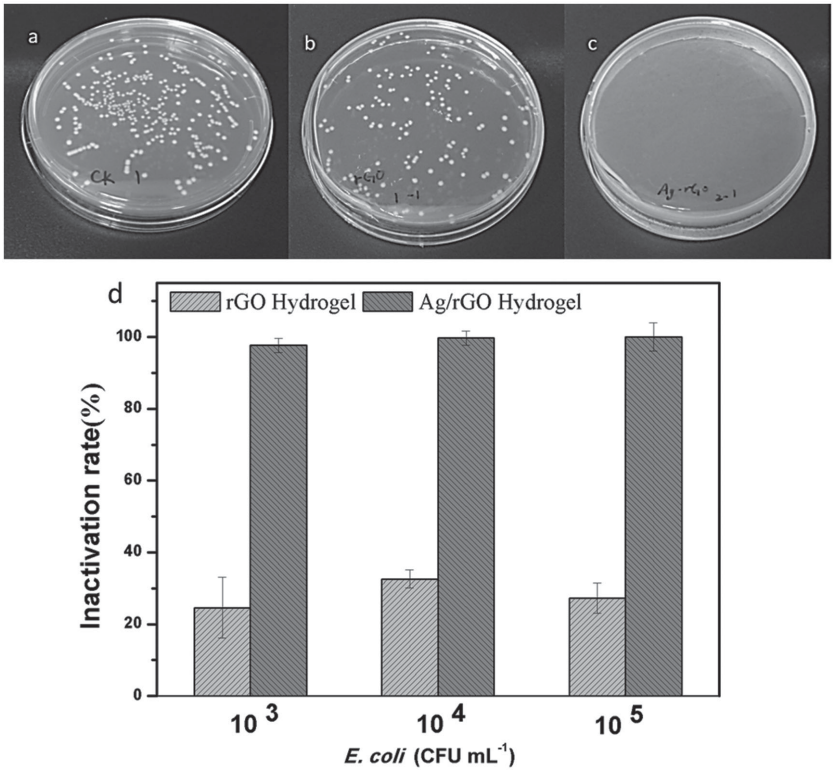

Figure 5. Photographs of colonies formed by *E. coli* cells in water samples: a) unfiltered, b) filtered through rGO hydrogel, c) filtered through Ag/rGO hydrogel, and d) *E. coli* inactivation rates achieved by rGO hydrogel and Ag/rGO hydrogel at different initial *E. coli* concentrations.

than its rGO counterpart. Silver has been known to be able to inactivate microorganism cells by destroying cell membrane and DNA replication.[26] Therefore it is not surprising that the antibacterial activity of rGO hydrogel is enhanced after silver nanoparticles are grafted on its porous stucture.

A simple filtration setup is harnessed to test the disinfection performance of the Ag/rGO hydrogel using bacteria suspension with an *Escherichia coli* concentration of 10^5 colony-forming units (CFU) mL^{-1} (Figure S5, Supporting Information). As the pore size of the Ag/rGO hydrogel is mostly in the range of micrometers, the filtration process can be driven by gravity, making it an ideal disinfection technology for POU water production. The average water flow rate in the test is 764 L h^{-1} m^{-2} and the hydraulic retention time of *E. coli* suspension in the Ag/rGO hydrogel is around 60 s. Representative results of the viability of *E. coli* cells in the effluent from rGO and Ag/rGO hydrogels are presented in **Figure 5**. Only around 35% of viable *E. coli* cells are inactivated after percolating though the rGO hydrogel, which is demonstrated by that many *E. coli* colonies are still formed (Figure 5b). By contrast, no viable *E. coli* colony remains on the agar plate for the effluent from the Ag/rGO hydrogel (Figure 5c), indicating that the *E. coli* cells are well inactivated. The disinfection performance of Ag/rGO hydrogels is closely linked to the ratio of $AgNO_3$/GO in the precursor as illustrated in Figure S6 (Supporting Information). With increasing the mass ratio of $AgNO_3$/GO from 0:1 to 1.5:1, *E. coli* inactivation ratio substantially increases. It is reasonable to gain better disinfection performance from Ag/rGO hydrogels prepared with more silver nitrate as more antibacterial Ag nanoparticles are present for inactivation. Based on the above results, Ag/rGO hydrogel prepared at a $AgNO_3$/GO ratio of 1.5:1 was selected for next studies.

The bactericidal performance of Ag/rGO hydrogel could also be related to the GO concentration as its pore size can be tuned by changing GO concentration.[14] Therefore, three Ag/rGO hydrogels were prepared with different concentrations of GO (0.5 mg mL^{-1}, 1 mg mL^{-1}, and 2 mg mL^{-1}, respectively) at a fixed amount of $AgNO_3$. However, the Ag/rGO hydrogel prepared using 0.5 mg mL^{-1} GO is readily to shrink (Figure S7, Supporting Information) and its mechanical strength is not enough for the water filtration process. The pore size of the Ag/rGO

hydrogel prepared using 2 mg mL^{-1} GO is smaller than that of the Ag/rGO hydrogel prepared using 1 mg mL^{-1} GO (Figure S8, Supporting Information). The bacterial disinfection results show that the two Ag/rGO hydrogels both achieve almost 100% of *E. coli* inactivation (Figure S9, Supporting Information). But the water flow rate slightly decreases to 611 L h^{-1} m^{-2} due to the small pore size, resulting in a longer hydraulic retention time of 75 s. The disinfection performance of the Ag/rGO hydrogel at different initial concentrations of *E. coli* cells was also evaluated. As shown in Figure 5d, high bacterial inactivation rates (>97%) can be achieved at the three initial concentrations of *E. coli* suspension (10^3, 10^4, and 10^5 CFU mL^{-1}), which indicates that the disinfection performance of the Ag/rGO hydrogel device is stable over a wide range of bacteria concentrations.

2.3. Key *E. coli* Inactivation Processes

To investigate the bactericidal mechanism of rGO and Ag/rGO hydrogels, two fluorescent nucleic acid dyes, 4, 6-diamidino-2-phenylindole (DAPI) and propidium iodide (PI), were employed to stain the DNA of *E. coli* cells. DAPI labels both live and dead cells while PI can only penetrate dead cells with compromised or damaged cell membranes.[27] **Figure 6**a shows that there are no cells stained by PI in untreated *E. coli*, indicating there are no dead cells due to damage of cell membrane. By contrast, some *E. coli* cells in the water sample filtered by rGO hydrogel can be stained by PI (Figure 6b), indicating that their cell membranes are destroyed by rGO nanosheets in the rGO hydrogel during filtration. The result is consistent with recent studies which also demonstrated that graphene nanosheet is able to cause inactivation of *E. coli* by membrane damage.[9,7b,28] For water sample filtered by Ag/rGO hydrogel, almost all *E. coli* cells are stained by PI, indicating that the *E. coli* inactivation is enhanced (Figure 6c). Both silver ions and silver nanoparticles have been reported to be a very effective disinfectant and can damage the cell membrane structures of *E. coli* cells.[26,29] Rod-shaped *E. coli* cells are usually around 2.0 μm long and 0.25–1.0 μm in diameter.[30] The large pores of Ag/rGO hydrogel (pore diameter >2 μm) allow *E. coli* cells to come into the pores and contact with Ag nanoparticles attached to the rGO during the filtration process, which might be the reason why high inactivation rate of *E. coli* is achieved by the Ag/rGO hydrogel.

The aforementioned results are further proven by the morphological studies of the bacteria before and after filtration using TEM. **Figure 7**a shows the internal structure of the untreated *E. coli* cells. It is clear that the cells have unanimous electron density, suggesting the cells are in a normal condition with intact cell walls and membranes.[26] Significant morphological changes occurred in *E. coli* cells after filtrating through the rGO and Ag/rGO hydrogels. As shown in Figure 7b, a small electron-light region occurs at the edge of the cell, indicating a partially damaged membrane surface induced by rGO nanosheets.[9,7b,28] It is known that graphene nanosheet could penetrate into cell membranes and extract large amounts of phospholipids due to the strong dispersion interactions between graphene and lipid molecules.[9] Moreover, GO sheets can also cover the *E. coli* cells, resulting in the cell viability loss.[31] Similar damage to the membrane of cells and cell viability loss might be also caused by the rGO hydrogel. For cells treated by the Ag/rGO hydrogel, more damage to cellular integrity is observed, demonstrated by larger electron-light regions near the membrane edges observed in the cells (Figure 7c), while some *E. coli* even lose their cytoplasm entirely (Figure 7d). This indicates that Ag/rGO hydrogel has better antibacterial ability due to the severe cell structure damage caused by both Ag nanoparticles and rGO nanosheets.

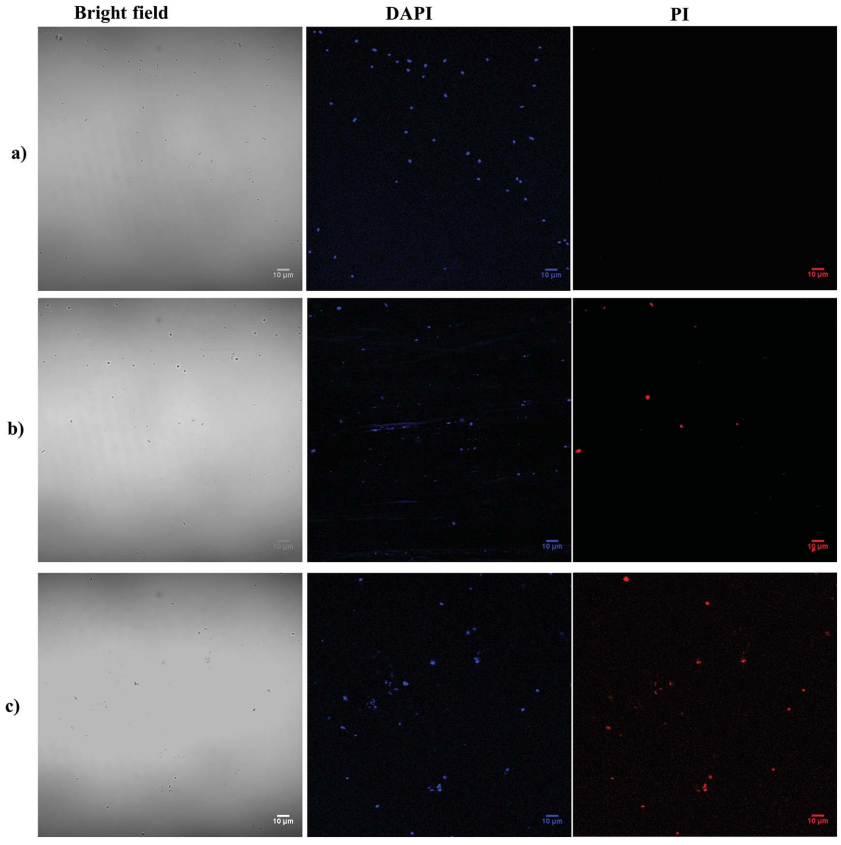

Figure 6. Confocal fluorescent images of live and dead *E. coli* cells in water samples: a) unfiltered, b) filtered through rGO hydrogel, and c) filtered through Ag/rGO hydrogel. Scale bar is 10 μm.

2.4. Effect of Leached Silver Ions on Bacterial Viability

Concentration of silver in the effluent was examined by inductively coupled plasma mass spectrometry (ICP-MS) to determine whether leached silver would pose a health risk. The analysis data show that the concentration of total silver in the effluent is only 7.33 ± 2.08 μg L^{-1}, far below the maximum con-

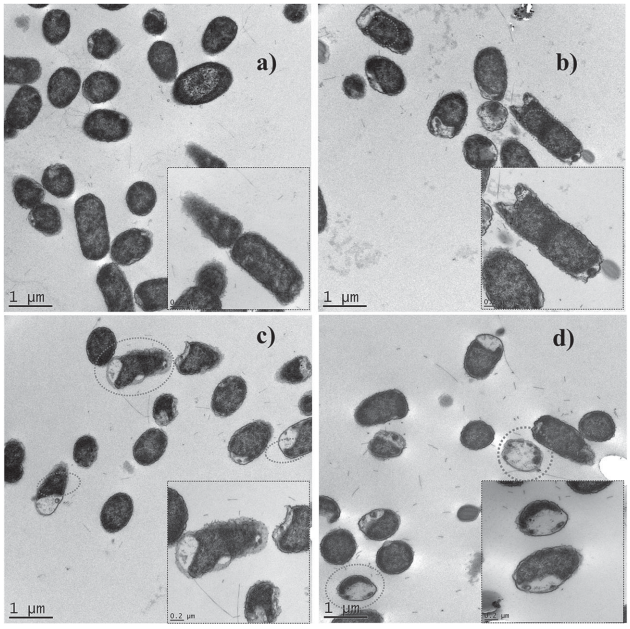

Figure 7. TEM images of *E. coli* cells in water samples: a) unfiltered, b) filtered through rGO hydrogel, and c,d) filtered through Ag/rGO hydrogel. Insets show representative cells at high magnification.

centration of silver in the drinking water standard (100 μg L^{-1}, US EPA drinking water guideline).[32] Such a low silver leaching level renders the Ag/rGO hydrogel a safe water purification device. The low silver leaching level from the hybrid hydrogel is in good agreement with the fact that silver nanoparticles are firmly attached to rGO nanosheets via the oxygen groups, evidenced by the FTIR spectra of the Ag/rGO hydrogel. To further exclude the possibility that the antibacterial activity is mainly contributed by the silver ions leached from Ag/rGO hydrogel, *E. coli* cells were treated by silver ion of 9 μg L^{-1}, same concentration as detected in the filtrate from Ag/rGO hydrogel. As shown in Figure S10 (Supporting Information), after 30 min treatment with silver ion, there are still 80% of viable cells. This result is not prominently different from that of the control group without silver ion, which means the leached silver ions in the effluent are not the primary disinfectants.

2.5. Feasibility for Natural Water Disinfection

The Ag/rGO hydrogel was also used for lake and creek water disinfection to test its feasibility for the practical treatment of real water. Results in **Table 1** show that *E. coli* in the lake and creek water samples is efficiently inactivated by Ag/rGO hydrogel, with *E. coli* inactivation rate of more than 94%. And for the coliforms, one commonly used bacterial indicator of sanitary quality of water,[33] Ag/rGO hydrogel kills around 99% of these bacteria. The flow rates under gravity feed for lake water (106.15 L h^{-1} m^{-2}) and creek water (127.38 L h^{-1} m^{-2}) are lower than that using synthetic bacteria suspension. The hydraulic retention time increases to 509 and 424 s for the two real water sources, respectively, due to the high concentration of sediment. Considering Ag/rGO hydrogel has good disinfection performances for coliforms and *E. coli*, it still shows promising potential for fast disinfection application if combined with some sediment pretreatment technologies.

3. Conclusion

Hybrid Ag/rGO hydrogels with dispersed Ag nanoparticles on rGO nanosheets and controlled macroporous network have been successfully fabricated using a facile hydrothermal reaction. In this strategy, Ag nanoparticles in Ag/rGO hydrogels not only enhance the antibacterial activity but also promote the forming of porous hydrogel. The Ag/rGO hydrogel, as a novel bactericidal filter, was then applied to water disinfection. Results showed Ag/rGO hydrogel could effectively kill more than 97% of viable *E. coli* cells with hydraulic retention time of 60 s via gravity filtration. When passing through Ag/rGO hydrogel, *E. coli* cells are inactivated due to cell structure damage induced by the bactericidal effects of both rGO nanosheets and Ag nanoparticles. Moreover, the leached silver from Ag/rGO hydrogel is below US EPA drinking water standard, suggesting that it could be a safe water purification device. This Ag/rGO hydrogel has also been tested for real lake and creek water disinfection, killing more than 94% *E. coli* cells and around 99% of coliforms, showing good feasibility for practical water disinfection. Consequently, the Ag/rGO hydrogel could be used for POU water disinfection and could provide safe drinking water in emergencies, especially in the aftermath of disasters when energy shortages and disinfection infrastructure deficiencies are critical.

4. Experimental Section

Synthesis: Graphene oxide (GO) colloid solution was prepared from graphite flakes (Sigma-Aldrich) according to the modified Hummer's method.[34] The obtained GO solution (2 mg mL^{-1}) was stored at room temperature and used for further experiments. To prepare Ag/rGO hydrogel, GO colloid solution (30 mL, 1 mg mL^{-1}) was prepared

Table 1. *E. coli* and coliform concentration in lake and creek water before and after filtered Ag/rGO hydrogels.

	Lake water			Creek water		
	Original	Treated	Inactivation rate	Original	Treated	Inactivation rate
E. coli [MPN/100 mL]	36.4 ± 15.4	<2.0	>94.51% ± 1.16%[a)]	153.6 ± 8.0	<2.0	>98.70% ± 0.04%[a)]
Coliforms [MPN/100 mL]	5308.9 ± 1437.6	15.1 ± 6.5	99.71% ± 0.12%[a)]	3295.6 ± 387.6	44.6 ± 23.8	98.71% ± 0.72%[a)]

[a)]The standard deviation of the inactivation rate was calculated by using the average and standard deviation of MPN numbers of three replicates based on the law of propagation of uncertainty.

by diluting GO stock solution with ultrapure water (>18 MΩ cm) and followed by ultrasonic treatment of 30 min. D-glucose (100 mg) and silver nitrate (0, 5, 15, 30, 45, and 60 mg) were then added into the GO solution under vigorous stirring. After 30 min of mixing, the solution was transferred into a Teflon-sealed autoclave and kept in an electronic oven at 120 °C for 20 h. The prepared hydrogels (Ag/rGO hydrogel) were washed with ultrapure water three times and then stored in pure water. The hydrogel without adding $AgNO_3$ was also washed with ultrapure water thrice and named pure rGO hydrogel.

Characterization: The morphologies of as-synthesized samples were characterized by scanning electron microscopy (SEM, FEI Nova NanoSEM 450) and transmission electron microscopy (TEM, FEI Tecnai G2 T20 TWIN). X-ray diffraction (XRD) patterns of samples were collected in the range of 3°–80° using a Rigaku Miniflex 600 X-ray diffract meter with Cu Ka radiation. Fourier transform infrared (FTIR) spectra were recorded with a Perkin-Elmer Frontier FT-IR/FIR Spectrometer.

Water Filtration Setup: The as-prepared hydrogels were inserted into a poly vinyl chloride (PVC) tube (diameter 10 mm), fixed by a perforated clamp hose fit and further sealed by waterproof gel (Figure S5, Supporting Information). A gravity-fed water filtration structure was then created by connecting this tube with a plastic funnel. Water contained *E. coli* was stored in the funnel and permeated the porous hydrogel driven by gravity. The flow rate was recorded and the hydraulic retention time was calculated by dividing the height of the hydrogel by the influent flow rate.

Testing Protocol for Disinfection Performance: E. coli (ATCC 11775), as an indicator for bacteria contamination in drinking water, was inoculated in Luria Bertani (LB) medium and cultured at 37 °C in a shaking water bath until the culture reached optical density of 0.5 at 600 nm. To prepare the bacterial solution for disinfection experiments, the cells were harvested by centrifugation and then diluted with sterile phosphate saline buffer solution (PBS, pH 7, 0.1 mol L^{-1}). PBS solution was spiked with *E. coli* at concentrations of 10^3, 10^4, and 10^5 colony-forming units (CFU) mL^{-1}. The prepared suspension (50 mL), a model for contaminated water, permeated the porous hydrogel by gravity without pressure or suction. After the filtration, 0.1 mL of the effluent (undiluted, three replicates) was collected and spread on LB agar plate and incubated at 37 °C for 18 h to form viable colony units. If all the replicates have no detectable colonies (but all positive controls were satisfied) then the number of colonies used for calculation was assumed to be <1/0.1 mL. *E. coli* concentrations in untreated water samples and the effluent of the pure rGO hydrogel were measured under the same conditions for comparison. For some samples, before plating, dilutions were done to make *E. coli* concentration at around 10^3 CFU mL^{-1}.

Fluorescent Imaging of Bacterial Suspensions: For the study of fluorescent imaging, the filtered effluents and untreated bacterial suspensions were firstly stained with a mixture of propidium iodide (PI, Sigma-Aldrich,1 μg mL^{-1}) and 4,6-diamidino-2-phenylindole (DAPI, Sigma-Aldrich, 5 μg mL^{-1}) for 10 min. Then they were centrifuged (8000 rpm, 5 min) and washed three times with sterile PBS solution. The samples were dropped on the microscope slides (5 μL for each sample), covered with a cover slip, and imaged using a Nikon C1 confocal microscope with a 60× objective.

TEM Images of E. coli Cells: For TEM imaging of *E. coli* cells, the treated and untreated cell pellets were collected by centrifugation (8000 rpm, 5 min) and fixed with 2.5% glutaraldehyde solution for 2 h at room temperature. Fixed cells were then treated by a protocol with serial steps in a PELCO BioWave microwave processor. Firstly, the samples were washed with 0.1 M sodium cacodylate buffer, then fixed with 1% aqueous OsO_4 (Fluka), and washed again twice with Milli-Q pure water. Cells were then dehydrated via acetone series (50%, 70%, 90%, 100%, and 100%, respectively) and embedded in Epon/Araldite resin (polymerization at 60 °C for 48 h). Ultrathin sections (around 70 nm) containing cells were placed on the grids, stained with uranyl acetate and lead citrate solution, and examined under the TEM (Hitachi H-7500).[9]

Effect of Leached Silver Ion on Bacterial Viability: Total silver concentration in the water samples treated by Ag/rGO hydrogels was measured by inductively coupled plasma mass spectrometry (ICP-MS) in a NATA-accredited laboratory (ALS Water Resources Group, Australia). To test the effect of leached silver ion on bacterial viability, an original ≈10^5 CFU mL^{-1} of *E. coli* suspension was divided into two aliquots. One aliquot was treated with 9 μg L^{-1} silver ion for 30 min; the other, treated with pure water, was used as control. The bacterial concentrations in both samples were measured using the aforementioned standard spread plating techniques.

Lake and Creek Water Disinfection: Two real-water samples were used, one from a lake in Clayton Campus of Monash University, Australia, and the other from Gardiners Creek in Yarra Catchment, Melbourne, Australia. Water samples of 50 mL were first filtrated by a cloth to remove large particles and then filtered by Ag/rGO hydrogels. Coliform/*E. coli* detection in the feed and filtrate was completed by using the Colilert-18/Quanti-Tray standard method with a dilution factor of 2. Three parallel samples were adopted for each experiment group.

Supporting Information

Supporting Information is available from the Wiley Online Library or from the author.

Acknowledgements

The authors acknowledge funding support by Australia Research Council (DP140103535). X. Zhang especially thanks Australian Research Council and Monash University for his ARF (DP110103533) and Larkins fellowships. The authors also thank Dr. Rebekah Henry and Ms Christelle Schang in EPHM Lab of Monash University for their kind help in accessing the *E. coli* culture and water sample collection and analysis. Louisa John-Krol is especially acknowledged for manuscript editing. The authors also acknowledge use of facilities within the Monash Centre for Electron Microscopy (MCEM) and Monash Micro Imaging (MMI).

Received: April 10, 2015
Revised: May 10, 2015
Published online: June 5, 2015

[1] W. H. Organization, *Emerging Issues in Water and Infectious Disease*, World Health Organization, Geneva **2003**.
[2] R. P. Schwarzenbach, B. I. Escher, K. Fenner, T. B. Hofstetter, C. A. Johnson, U. Von Gunten, B. Wehrli, *Science* **2006**, *313*, 1072.
[3] S.-L. Loo, A. G. Fane, W. B. Krantz, T.-T. Lim, *Water Res.* **2012**, *46*, 3125.
[4] T. A. Dankovich, D. G. Gray, *Environ. Sci. Technol.* **2011**, *45*, 1992.
[5] S.-L. Loo, A. G. Fane, T.-T. Lim, W. B. Krantz, Y.-N. Liang, X. Liu, X. Hu, *Environ. Sci. Technol.* **2013**, *47*, 9363.
[6] P. V. Kamat, *J. Phys. Chem. Lett.* **2009**, *1*, 520.
[7] a) O. Akhavan, E. Ghaderi, *ACS Nano* **2010**, *4*, 5731; b) S. Liu, T. H. Zeng, M. Hofmann, E. Burcombe, J. Wei, R. Jiang, J. Kong, Y. Chen, *ACS Nano* **2011**, *5*, 6971.
[8] a) M. Sawangphruk, P. Srimuk, P. Chiochan, T. Sangsri, P. Siwayaprahm, *Carbon* **2012**, *50*, 5156; b) K. Krishnamoorthy, M. Veerapandian, L.-H. Zhang, K. Yun, S. J. Kim, *J. Phys. Chem. C* **2012**, *116*, 17280; c) J. Li, G. Wang, H. Zhu, M. Zhang, X. Zheng, Z. Di, X. Liu, X. Wang, *Sci. Rep.* **2014**, *4*, 4359.
[9] Y. Tu, M. Lv, P. Xiu, T. Huynh, M. Zhang, M. Castelli, Z. Liu, Q. Huang, C. Fan, H. Fang, R. Zhou, *Nat. Nanotechnol.* **2013**, *8*, 594.
[10] Z. Niu, L. Liu, L. Zhang, X. Chen, *Small* **2014**, *10*, 3434.
[11] a) M. R. Das, R. K. Sarma, R. Saikia, V. S. Kale, M. V. Shelke, P. Sengupta, *Colloids Surf. B: Biointerfaces* **2011**, *83*, 16; b) Q. Bao,

D. Zhang, P. Qi, *J. Colloid Interface Sci.* **2011**, *360*, 463; c) W.-P. Xu, L.-C. Zhang, J.-P. Li, Y. Lu, H.-H. Li, Y.-N. Ma, W.-D. Wang, S.-H. Yu, *J. Mater. Chem.* **2011**, *21*, 4593.
[12] Q. Li, S. Mahendra, D. Y. Lyon, L. Brunet, M. V. Liga, D. Li, P. J. Alvarez, *Water Res.* **2008**, *42*, 4591.
[13] J. M. Phillips, *MRS Bull.* **2006**, *31*, 45.
[14] Z. Tang, S. Shen, J. Zhuang, X. Wang, *Angew. Chem.* **2010**, *122*, 4707; *Angew. Chem. Int. Ed.* **2010**, *49*, 4603.
[15] C. Li, G. Shi, *Adv. Mater.* **2014**, *26*, 3992.
[16] Y. Wang, X. Yang, L. Qiu, D. Li, *Energy Environ .Sci.* **2013**, *6*, 477.
[17] E. Wang, M. S. Desai, S.-W. Lee, *Nano Lett.* **2013**, *13*, 2826.
[18] K. Bahartan, J. Gun, S. Sladkevich, P. V. Prikhodchenko, O. Lev, L. Alfonta, *Chem. Commun.* **2012**, *48*, 11957.
[19] Z. Fan, B. Liu, J. Wang, S. Zhang, Q. Lin, P. Gong, L. Ma, S. Yang, *Adv. Funct. Mater.* **2014**, *24*, 3933.
[20] J. Ma, J. Zhang, Z. Xiong, Y. Yong, X. Zhao, *J. Mater. Chem.* **2011**, *21*, 3350.
[21] S. K. Li, Y. X. Yan, J. L. Wang, S. H. Yu, *Nanoscale* **2013**, *5*, 12616.
[22] V. H. Pham, T. V. Cuong, S. H. Hur, E. Oh, E. J. Kim, E. W. Shin, J. S. Chung, *J. Mater. Chem.* **2011**, *21*, 3371.
[23] X.-Z. Tang, X. Li, Z. Cao, J. Yang, H. Wang, X. Pu, Z.-Z. Yu, *Carbon* **2013**, *59*, 93.
[24] H. Wang, J. T. Robinson, G. Diankov, H. Dai, *J. Am. Chem. Soc.* **2010**, *132*, 3270.
[25] Y. Xu, K. Sheng, C. Li, G. Shi, *ACS Nano* **2010**, *4*, 4324.
[26] W.-R. Li, X.-B. Xie, Q.-S. Shi, H.-Y. Zeng, O.-Y. You-Sheng, Y.-B. Chen, *Appl. Microbiol. Biotechnol.* **2010**, *85*, 1115.
[27] J. Tang, Q. Chen, L. Xu, S. Zhang, L. Feng, L. Cheng, H. Xu, Z. Liu, R. Peng, *ACS Appl. Mater. Interfaces* **2013**, *5*, 3867.
[28] Y. Li, H. Yuan, A. von dem Bussche, M. Creighton, R. H. Hurt, A. B. Kane, H. Gao, *Proc. Natl. Acad. Sci. U.S.A.* **2013**, *110*, 12295.
[29] Q. Feng, J. Wu, G. Chen, F. Cui, T. Kim, J. Kim, *J. Biomed. Mater. Res.* **2000**, *52*, 662.
[30] R. J. Kadner, Bacteria: Diversity of structure of bacteria, http://www.britannica.com/EBchecked/topic/48203/bacteria/39334/Diversity-of-structure-of-bacteria (accessed: October 2014).
[31] S. Liu, M. Hu, T. H. Zeng, R. Wu, R. Jiang, J. Wei, L. Wang, J. Kong, Y. Chen, *Langmuir* **2012**, *28*, 12364.
[32] W. H. Organization, *Guidelines for Drinking-Water Quality: First Addendum to Volume 1, Recommendations* Vol. *1*, World Health Organization **2006**, Ch. 12.
[33] A. Rompré, P. Servais, J. Baudart, M.-R. de-Roubin, P. Laurent, *J. Microbiol. Methods* **2002**, *49*, 31.
[34] W. S. Hummers Jr., R. E. Offeman, *J. Am. Chem. Soc.* **1958**, *80*, 1339.